Optics and Laser Technology 99 (2018) 315–325

Contents lists available at ScienceDirect

Optics and Laser Technology

journal homepage: www.elsevier.com/locate/optlastec

Full length article

Effects of momentum transfer on sizing of current collectors for lithium-ion batteries during laser cutting

Dongkyoung Lee [a,*], Jyotirmoy Mazumder [b,c]

[a] Department of Mechanical and Automotive Engineering, Kongju National University, Cheonan 31080, South Korea
[b] Center for Lasers and Plasmas for Advanced Manufacturing (CLPAM), Department of Mechanical Engineering, University of Michigan, Ann Arbor, MI 48109, USA
[c] Department of Material Science and Engineering, University of Michigan, Ann Arbor, MI 48109, United States

ARTICLE INFO

Article history:
Received 14 June 2017
Received in revised form 22 August 2017
Accepted 6 September 2017
Available online 20 September 2017

Keywords:
Laser cutting
Lithium-ion battery
Current collector
Copper
Aluminum
Numerical simulation

ABSTRACT

One of the challenges of the lithium-ion battery manufacturing process is the sizing of electrodes with good cut surface quality. Poor cut surface quality results in internal short circuits in the cells and significant heat generation. One of the solutions that may improve the cut quality with a high cutting speed is laser cutting due to its high energy concentration, fast processing time, high precision, small heat affected zone, flexible range of laser power and contact free process. In order to utilize the advantages of laser electrode cutting, understanding the physical phenomena for each material is crucial. Thus, this study focuses on the laser cutting of current collectors, such as pure copper and aluminum. A 3D self-consistent mathematical model for the laser cutting, including fluid flow, heat transfer, recoil pressure, multiple reflections, capillary and thermo-capillary forces, and phase changes, is presented and solved numerically. Simulation results for the laser cutting are analyzed in terms of penetration time, depth, width, and absorptivity, based on these selected laser parameters. In addition, melt pool flow, melt pool geometry and temperature distribution are investigated.

1. Introduction

Over the last decade, battery technology has attracted much attention due to a high demand for clean energy sources of portable electronic devices and automobiles. In particular, the automotive industry utilizes batteries not only for the hybridization of gasoline and diesel engines, called hybrid electric vehicles (HEVs), but also for developing electric vehicles (EVs) due to the strict requirements of environmentally friendly propulsion systems [1]. Of the many available battery technologies, the lithium-ion battery has been identified as the most promising battery technology for electric-drive vehicles, because of its superior performance [1]. Battery performance can be highly affected by the coating materials on its electrodes [2–7]. In addition, manufacturing processes of lithium-ion batteries are also an important factor that influence battery performance [1,8,9].

In the lithium-ion battery manufacturing process, the current collectors (copper and aluminum) are coated with active electrode materials, which are graphite and lithium metal oxides such as $LiCoO_2$, $LiMn_2O_4$, and $LiFePO_4$, as shown in Fig. 1. After that, electrodes need to be cut to different sizes. Currently, electrodes are sized using mechanical cutting by rotary knives and dies. Mechanical cutting results in a cut surface of poor cut quality, with delamination, burrs, and edge bending. This poor cut quality may give rise to internal short circuits in the cells. In addition to internal shorts, significant heat generation and possible thermal runaway are possible when the cells are in use. Laser cutting is a promising solution to improve electrode cut quality with high cutting speed due to its high energy concentration, fast processing time, high precision, small Heat Affected Zone (HAZ), flexible range of laser power, and contact free process [10–13]. Furthermore, properly manipulated material melting prevents a high level of distortion and warp, which is typically present in mechanical cutting [10]. However, to fully utilize these advantages for laser cutting of the electrodes, an understanding of the underlying physical phenomena is essential.

Laser cutting involves phase changes such as solidification, melting, and evaporation. A high evaporation speed forms the region where the continuum hypothesis fails, called the Knudsen layer, on the Liquid-Vapor (L/V) interface [9,14–16]. Furthermore, a deep penetration hole is observed prior to completing the cutting, which requires full penetration of the materials. Laser energy can accumulate inside a deep penetration hole by multiple reflections so that absorbed energy increases significantly. This increased energy absorption in turn expedites the penetration of

* Corresponding author.
E-mail address: ldkkinka@kongju.ac.kr (D. Lee).

http://dx.doi.org/10.1016/j.optlastec.2017.09.016
0030-3992/

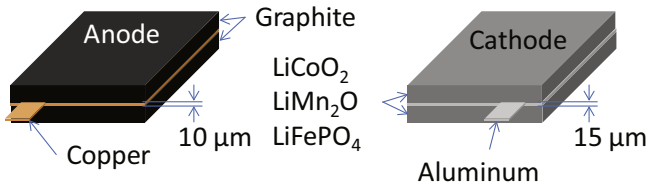

Fig. 1. Configuration of electrodes.

the hole. Due to these physical characteristics, laser cutting promises cleaner, clearer, sharper edges compared to conventional mechanical cutting [4–7,9,12,17–21].

The melt pool and heat flows, as well as intensity and pressure distributions during the laser cutting, are major factors affecting process quality. Many researchers have worked to understand the influence of these physical phenomena on laser-material interaction. Chan and Mazumder [22] developed a simple one-dimensional steady-state laser-material interaction model. They examined the damage caused by vaporization and liquid expulsion. This mathematical model evolved to two- and three-dimensions. A two-dimensional model was developed not only for investigating material damage owing to melting and vaporization [23], but also for analyzing effects of assist gas and multiple reflections inside the cavity [24]. Ki et al. [25–30] developed a mathematical three-dimensional self-consistent laser-material interaction model with the aid of the level-set method. These studies included fluid flow, heat transfer, solidification, melting, evaporation, multiple internal reflections, free surface evolution, and surface forces on mild steel.

The understanding of physical phenomena for each material during the laser cutting is an essential step prior to investigating laser cutting of electrodes. In this study, pure copper and aluminum are chosen as an initial context to achieve laser cutting of the current collectors for lithium-ion batteries. Numerical studies of laser processing parameters on current collectors for lithium-ion batteries have been done by Lee et al. [21]. They found thresholds of laser processing parameters such as laser power and scanning speed. However, details of physical phenomena during the laser cutting are not provided. Therefore, this paper focuses on the understanding of physical phenomena during the laser cutting of current collectors. This paper is organized as follows.

First, a theoretical model of three-dimensional self-consistent laser cutting is described for pure copper and aluminum. Second, simulation results for the laser cutting are analyzed in terms of penetration time, depth, width, and absorptivity, based on the selected laser parameters. In addition, melt pool flow, melt pool geometry and temperature distribution are investigated at selected moments in three-dimensions. Finally, the conclusions drawn from this work are summarized.

2. Mathematical modeling

2.1. Governing equations

This study assumes an incompressible, laminar and Newtonian liquid flow. Vaporization processes are treated as the volume source. Continuity, momentum transfer, energy transfer can be expressed by following governing equations.

$$\nabla \cdot \mathbf{u} = \frac{\dot{m}''_{evap}}{\rho}\delta(\phi) \tag{1}$$

$$\frac{\partial(\rho u)}{\partial t} + \nabla\cdot(\rho \mathbf{u} u) = \nabla\cdot\left(\mu_l \frac{\rho}{\rho_l}\nabla u\right) - \frac{\mu_l}{K}\frac{\rho}{\rho_l}u - \frac{\partial p}{\partial x} - \mathbf{e_x}\cdot\left(\sigma n\kappa - \Delta_s T\frac{d\sigma}{dT}\right)\delta(\phi) \tag{2}$$

$$\frac{\partial(\rho v)}{\partial t} + \nabla\cdot(\rho \mathbf{u} v) = \nabla\cdot\left(\mu_l \frac{\rho}{\rho_l}\nabla v\right) - \frac{\mu_l}{K}\frac{\rho}{\rho_l}v - \frac{\partial p}{\partial y} - \mathbf{e_y}\cdot(\sigma n\kappa - \Delta_s T\frac{d\sigma}{dT})\delta(\phi) \tag{3}$$

$$\frac{\partial(\rho w)}{\partial t} + \nabla\cdot(\rho \mathbf{u} w) = \nabla\cdot\left(\mu_l \frac{\rho}{\rho_l}\nabla w\right) - \frac{\mu_l}{K}\frac{\rho}{\rho_l}w - \frac{\partial p}{\partial z} - \mathbf{e_z}\cdot\left(\sigma n\kappa - \Delta_s T\frac{d\sigma}{dT}\right)\delta(\phi) \tag{4}$$

$$\frac{\partial(\rho \bar{C}_{pl} T)}{\partial t} + \mathbf{u}\cdot\nabla(\rho \bar{C}_{pl} T) = \nabla\cdot(k\nabla T) - L\frac{\partial(\rho f_l)}{\partial t} + \frac{\partial(\rho f_s \Delta \bar{C}_p T)}{\partial t} + \dot{q}''(t,\mathbf{x})\delta(\phi) \tag{5}$$

where $\mathbf{u}$ is the liquid velocity vector, $\mathbf{x}$ is the spatial vector, ρ is the density, μ is the viscosity, p is the pressure, k is the thermal conductivity, $\bar{C}_{pl}$ is the average-specific heat of liquid, t is the time, f_l is the liquid mass fraction and $\delta(\phi)$ is the delta function to incorporate boundary conditions of the L/V interface. The phase interactions are considered as a porous media. To describe porous media, it was assumed that permeability K is varying with the liquid volume fraction, according to the Kozeny-Carman Equation [31].

$$K = K_0\frac{g_l^3}{(1-g_l)^2} \tag{6}$$

Fourth terms on the right hand side of Eqs. (2)–(4) are boundary conditions for the L/V interface. This model contains both the capillary and thermo-capillary forces similar to Ki et al. [30]. The second and third terms on the right hand side of Eq. (5) are the boundary conditions for energy equations on the S/L interface. This is adopted from Bennon's continuum model [32]. The solid mass fraction is defined as

$$f_s = 1 - f_l \tag{7}$$

Similarly, the volume fraction can be defined for liquid and solid (g_l and g_s). The relationship between the mass fraction (f_l) and the volume fraction (f_s) can be described as

$$f_s = \frac{\rho_s g_s}{\rho} \tag{8}$$

$$f_l = \frac{\rho_l g_l}{\rho} \tag{9}$$

$$g_s + g_l = 1 \tag{10}$$

with these relations, the density (ρ), thermal conductivity (k), and enthalpy (h) for the liquid and solid mixture are defined as

$$\rho = g_s\rho_s + g_l\rho_l \tag{11}$$

$$k = \left(\frac{g_s}{k_s} + \frac{g_l}{k_l}\right)^{-1} \tag{12}$$

$$h = f_s h_s + f_l h_l \tag{13}$$

This model assigns the mass liquid fraction 1 and 0 when the temperature is above and below melting temperature, respectively. This is because pure materials have been selected. The phase enthalpies are obtained as

$$h_s = \int_0^T C_{ps}dT \tag{14}$$

$$h_l = \int_0^{T_m} C_{ps}dT + L_m + \int_{T_m}^T C_{pl}dT \tag{15}$$